Supplemental material

Gratia et al., https://doi.org/10.1084/jem.20181329

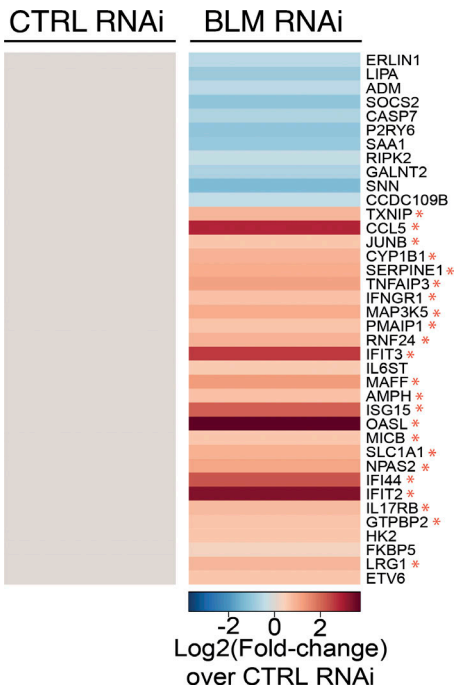

Figure S1. **BLM RNAi in HeLa cells induces an ISG signature.** Heatmaps representing the $\log_2$ fold-change of the normalized expression values of 38 differentially expressed genes between control (CTRL RNAi) and BLM-depleted (BLM RNAi) HeLa cells. ISGs previously recognized in another study (Schoggins et al., 2011) are highlighted by red asterisks.

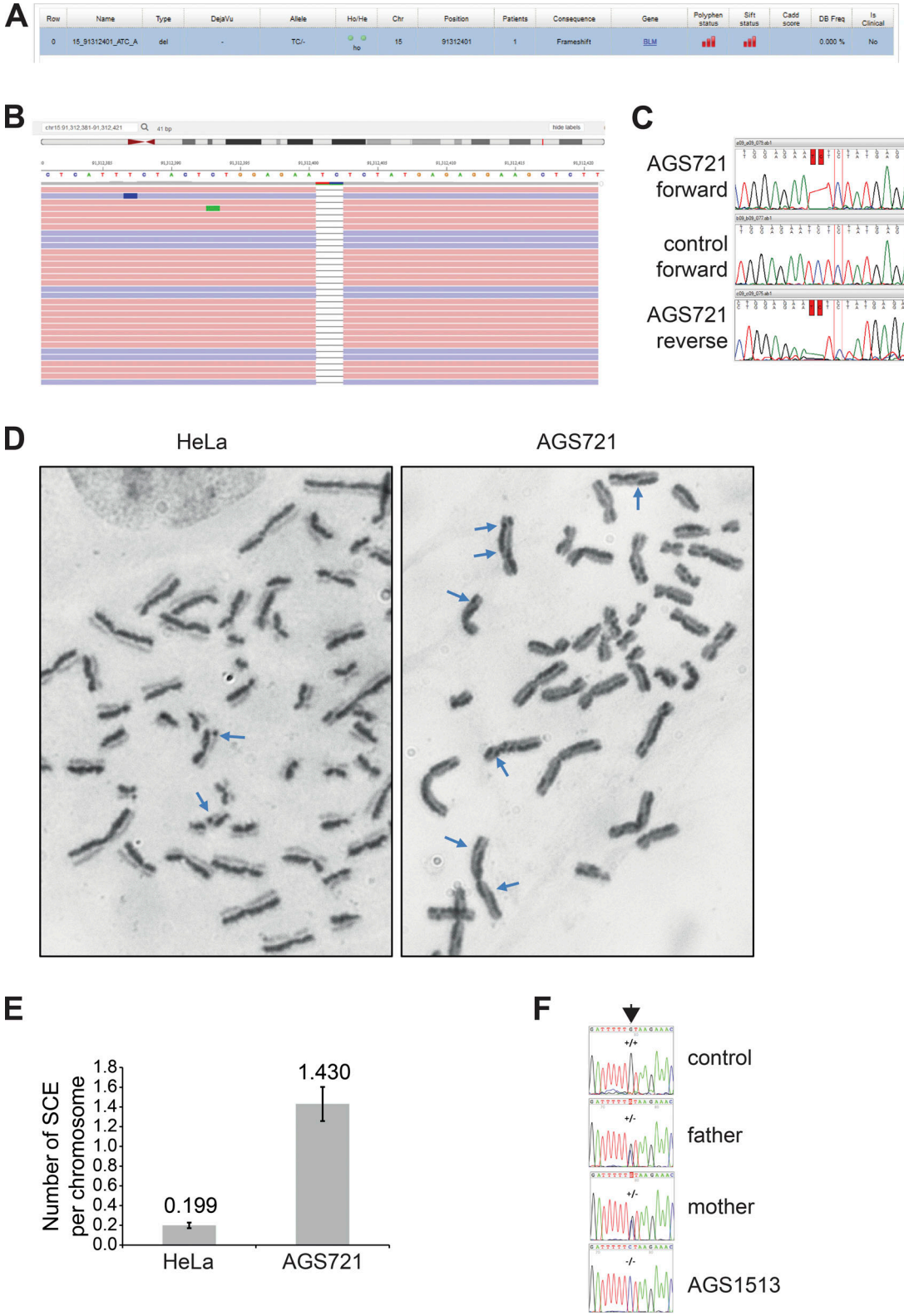

Figure S2. ***BLM* mutations in patients AGS721 and AGS1513. (A)** Whole-exome sequencing–based identification of the AGS721 homozygous mutation; screen capture from the results window of the Polyweb software (http://www.polyweb.fr) using the following criteria: frequency in public databases <0.001%; recessive; coding. **(B)** Screen capture of the AGS721 mutation coverage using IGV software. **(C)** Electropherogram of *BLM* cDNA from peripheral blood mononuclear cells of AGS721, illustrating the homozygous deletion of two nucleotides. **(D)** SCE frequency in HeLa cells and SV40-immortalized AGS721 cells; representative images; examples of exchanges are indicated with arrows. **(E)** Quantification of SCE frequency in HeLa cells (adapted from Lahkim Bennani-Belhaj et al., 2010) and AGS721 cells (n = 338 chromosomes analyzed; mean with SD). **(F)** Electropherogram of *BLM* cDNA of AGS1513, parents, and unrelated control.

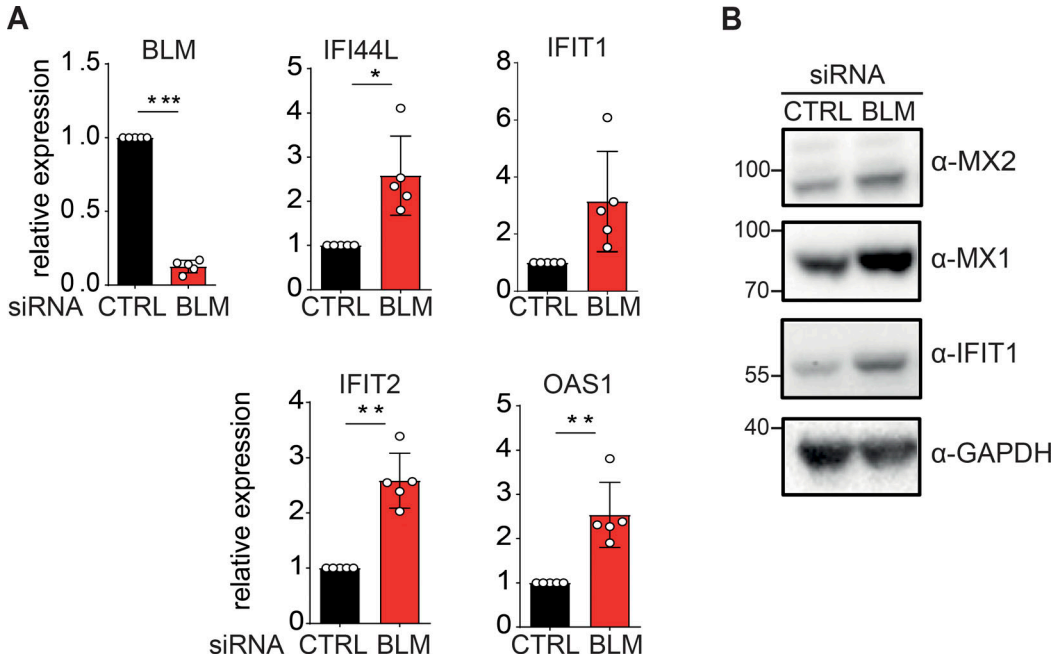

Figure S3. **BLM depletion induces ISGs in an independent source of primary human fibroblasts. (A)** mRNA level expression of *BLM*, *IFI44L*, *IFIT1*, *IFIT2*, and *OAS1* determined by RT-qPCR in an independent source of primary human fibroblasts treated with control (CTRL) or BLM siRNA for 72 h (mean with SD of $n = 5$ independent experiments; one-sample *t* test, *P < 0.05, **P < 0.01, ***P < 0.001). **(B)** Protein levels of *MX2*, *MX1*, *IFIT1*, and *GAPDH* in cells, as in Fig. S2 A (representative of $n = 5$ independent experiments).

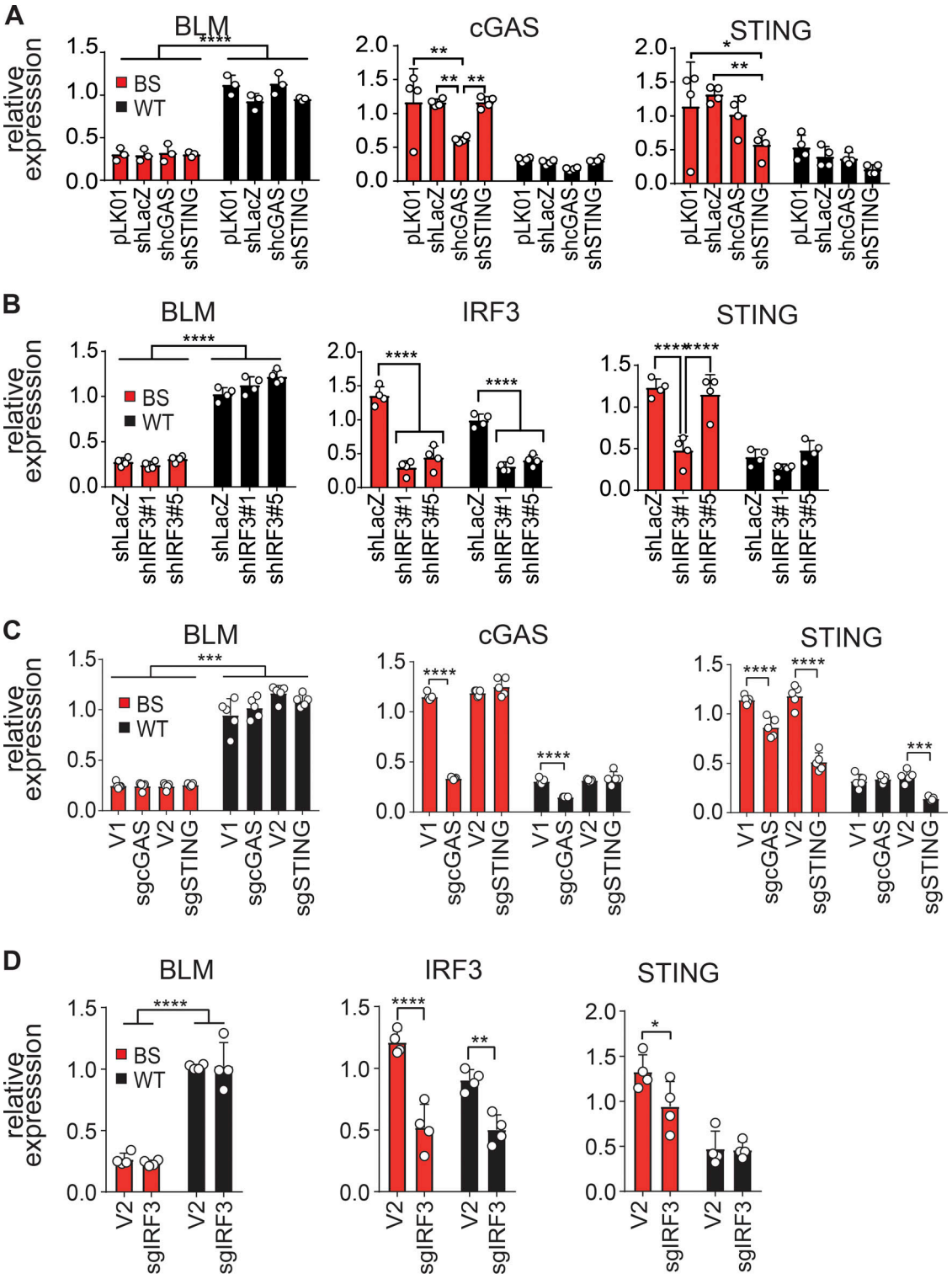

Figure S4. **ISG signature induction in BS cells requires the cGAS–STING–IRF3 pathway. (A)** mRNA level expression of *BLM*, *cGAS*, and *STING* in cells, as in Fig. 3 A (mean with SD of *n* = 4 independent experiments; two-way ANOVA with Tukey post-test, *P < 0.05, **P < 0.01, ****P < 0.0001). **(B)** mRNA level expression of *BLM*, *IRF3*, and *STING* in cells, as in Fig. 3 A (mean with SD of *n* = 4 independent experiments; two-way ANOVA with Tukey post-test, ****P < 0.0001). **(C)** mRNA level expression of *BLM*, *cGAS*, and *STING* in cells, as in Fig. 3 D (mean with SD of *n* = 5 independent experiments; two-way ANOVA with Tukey post-test, ***P < 0.001, ****P < 0.0001). **(D)** mRNA level expression of *BLM*, *IRF3*, and *STING* cells, as in Fig. 3 D (mean with SD of *n* = 4 independent experiments; two-way ANOVA with Sidak post-test, *P < 0.05, **P < 0.01, ****P < 0.0001).

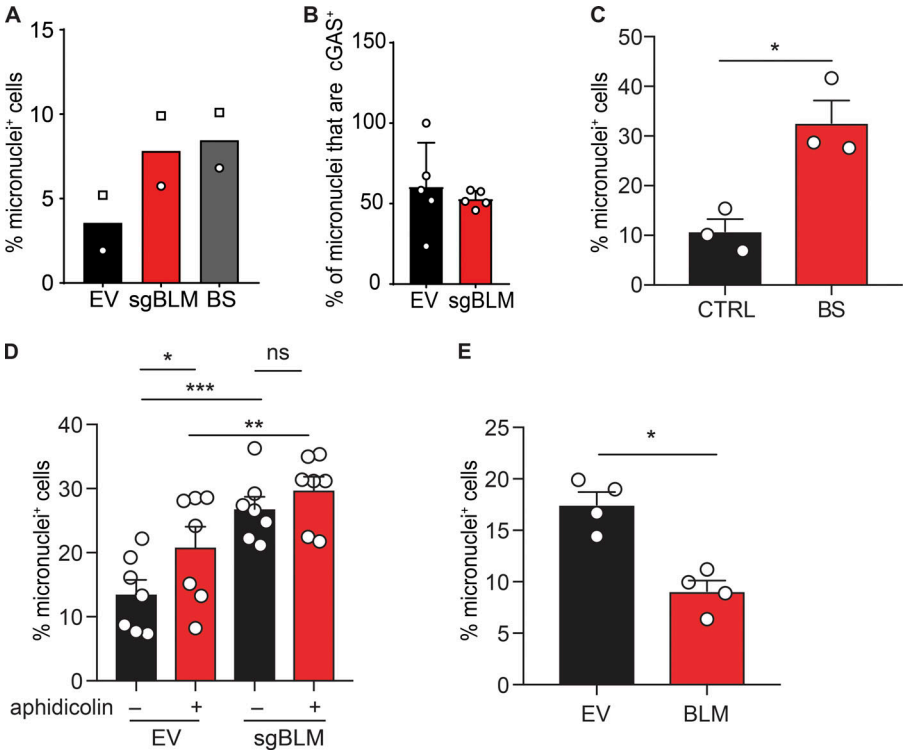

Figure S5. **BLM deficiency increases the frequency of micronuclei positive for cGAS. (A)** Frequency of cells positive for at least one micronucleus in SV40-immortalized control (EV) or *BLM*-knockout (sgBLM) fibroblasts and BS fibroblasts. Data are the combination of two independent experiments. **(B)** Percentage of micronuclei that are GFP-cGAS positive in cells, as in Fig. 5 A (mean with SD of $n = 5$ combined independent experiments). **(C)** Frequency of cells positive for at least one micronucleus in primary control (CTRL) or BLM-deficient fibroblasts (BS; mean with SEM of $n = 3$ combined independent experiments; paired t test, $^*P < 0.05$). **(D)** Frequency of cells positive for at least one micronucleus in SV40-immortalized control (EV) or *BLM*-knockout fibroblasts (sgBLM) and treated by aphidicolin (mean with SEM of $n = 7$ combined independent experiment, treatment with 12 or 30 µM in four and three experiments respectively; repeated measures one-way ANOVA with a Sidak post-test, $^*P < 0.05$, $^{**}P < 0.01$, $^{***}P < 0.01$). **(E)** Frequency of cells positive for at least one micronucleus in SV40-immortalized control BS cells or BLM-transduced BS fibroblasts, as in Fig. 1 D (mean with SEM of $n = 4$ combined independent experiments; paired t test, $^*P < 0.05$).

Table S1. **Mutations and clinical features of patients in the study**

Patient	Mutation	Case history
AGS721	Homozygous c.2349_2350del/p.Tyr784*	This male child was born to unrelated parents with no family history of neurological or immunological problems. The pregnancy was complicated by intrauterine growth retardation and he was delivered at 36 wk of gestation weighing 1 kg. There was poor feeding from the outset so that he required a nasogastric tube for 2 yr.
		The first year of life was complicated by mild global developmental delay, walking at 18 mo of age. His mobility was best around the age of 3 yr, but this was followed by progressive lower limb spasticity, pyramidal signs, and toe walking, so that he was diagnosed with a progressive spastic paraplegia. His upper limbs were less affected, although he showed mild problems with fine motor control. He experienced two episodes of pneumonia at age 18 mo and 3 yr. He continued to exhibit mild learning difficulties, with poor ongoing growth (height, weight, and head circumference less than the third centile). He had micrognathia and osteoporosis with evidence of vertebral crush fractures so that he required vitamin D supplementation and bisphosphonate therapy. Erythrocyte sedimentation rate was persistently raised (22–80 mm/h; normal, <20), with low IgG and IgM, raised CSF neopterin (58 pmol/liter; normal, <30) but normal lymphocyte subsets. Brain MRI showed mild nonspecific abnormal high signal in the white matter.
		At the age of 8 yr, he was started on intravenous immunoglobulin replacement at 0.4 g/kg, given four times weekly. His progressive spastic paraplegia plateaued from 10 yr of age, but he has experienced orthopedic complications with kyphoscoliosis, requiring femur osteotomy and adductor releases at age 12 yr.
AGS1513	Homozygous c.3164G>C/p.C1055S	This male was the first-born child to a nonconsanguineous couple of Portuguese origin. There was no family history of note. Intrauterine growth retardation recognized during the second trimester of pregnancy prompted fetal karyotyping, which was normal. He was delivered at 38 wk of gestation with a birth weight, height, and head circumference of 2,160 g, 43 cm, and 32 cm, respectively. A congenital nevus of the buttocks was surgically resected and identified as a dermal nevus with neuroid differentiation/features of a schwannoma on histology.
		Psychomotor development was considered as normal. However, at 20 mo of age, growth hormone therapy was introduced because of short stature (weight, height, and head circumference < −3 SDs). Growth indices then improved, so that he had achieved a normal weight (−0.5 SD) and height (−1.5 SD) within 6 mo, while he remained microcephalic (−3.5 SDs). Examination at this age identified multiple hyperpigmented and hypopigmented skin patches and mild facial dysmorphism with triangular face and thin upper lip.
		At 5 yr of age, he exhibited erythematous lesions of the face and legs following sun exposure. A diagnosis of BS was made on exome sequencing and growth hormone therapy discontinued because of an increased cancer risk. At last examination, aged 8 yr, he weighed 27.6 kg (+0.5 SD), with a height of 118 cm (−1.5 SD). He has experienced frequent ear, nose, and throat infections and recurrent episodes of fever. IgM and IgG are low. He is of normal intellect and attends regular school.

MRI, magnetic resonance imaging.

Table S2. **Plasmids used in the study**

Plasmid name	Description	Sequence inserted
pCMV-VSVG	VSVG envelope protein	–
psPAX2	Viral protein for lenti production	–
pTRIP-CMV-Puro2A	EV for gene expression (puromycin resistant)	–
pTRIP-CMV-Puro2A-BLM	Vector for BLM expression (puromycin resistant)	*BLM* ORF
pTRIP-CMV-EGFP-FLAG-cGAS E225A-D227A	Vector for cGAS expression (Ntase mutant)	*cGAS* ORF mutation E225A-D227A
pLKO.1-puro	EV for shRNA silencing (puromycin resistant)	
pLKO.1-puro-shLACZ	Vector with shLacZ control (puromycin resistant)	5′-GCGATCGTAATCACCCGAGTG-3′
		5′-CTCGAG-3′
		5′-CACTCGGGTGATTACGATCGC-3′
pLKO.1-puro-cGASsh4	Vector with shcGAS (puromycin resistant)	5′-CAACTACGACTAAAGCCATTT-3′
		5′-CTCGAG-3′
		5′-AAATGGCTTTAGTCGTAGTTG-3′
pLKO.1-puro-STING-sh5	Vector with shSTING (puromycin resistant)	5′-GCCCGGATTCGAACTTACAAT-3′
		5′-CTCGAG-3′
		5′-ATTGTAAGTTCGAATCCGGGC-3′
pLKO.1-puro-irf3-shrna1	Vector with shIRF3 #1 (puromycin resistant)	5′-CTGCCTGGATGGCCAGTCACAC-3′
		5′-CTGTGAAGCCACAGATGGG-3′
		5′-GTGTGACTGGCCATCCAGGCAG-3′
pLKO.1-puro-irf3-shrna5	Vector with shIRF3 #2 (puromycin resistant)	5′-TACCCAGGAAGACATTCTGGAT-3′
		5′-CTGTGAAGCCACAGATGGG-3′
		5′-ATCCAGAATGTCTTCCTGGGTA-3′
pLCRISPR-CMV	EV for gene silencing by CRISPR (puromycin resistant)	–
pLCRISPR-CMV-cGAS3	Vector for cGAS silencing by CRISPR (puromycin resistant)	5′-GGGATCCCGACTTCCTGGCG-3′
pLentiCRISPRv2	EV for gene silencing by CRISPR (puromycin resistant)	–
pLentiCRISPRv2-STING_gRNA3	Vector for STING silencing by CRISPR (puromycin resistant)	5′-AGGTACCGGAGAGTGTGCTC-3′
pLentiCRISPRv2 sgIRF3#5	Vector for IRF3 silencing by CRISPR (puromycin resistant)	5′-GAAGCGGCTGTTGGTGCCGG-3′
pLentiCRISPRv2 sgBLM10	Vector for BLM silencing by CRISPR (puromycin resistant)	5′-GGAACGAACTGCTTCAGCAG-3′
pLentiCRISPRv2 Neo	EV for gene silencing by CRISPR (neomycin resistant)	–
pLentiCRISPRv2 Neo sgTREX1	Vector for TREX1 silencing by CRISPR (neomycin resistant)	5′-GAGAGCTTGTCTACCACACG-3′

ORF, open reading frame.

Table S3. **siRNAs used in the study**

Nontargeting siRNA pool	siBLM pool
5′-UGGUUUACAUGUCGACUAA-3′	5′-CUAAAUCUGUGGAGGGUUA-3′
5′-UGGUUUACAUGUUGUGUGA-3′	5′-GAUCAAUGCUGCACUGCUU-3′
5′-UGGUUUACAUGUUUUCUGA-3′	5′-GGAUGACUCAGAAUGGUUA-3′
5′-UGGUUUACAUGUUUUCCUA-3′	5′-GCAACUAGAACGUCACUCA-3′

Table S4. **Primers used in the study**

	Forward	Reverse
BLM	5′-CTGATGCCGACTGGAGGTG-3′	5′-TGACAACAGTGACCCCAGGA-3′
Actin	5′-CTGGAACGGTGAAGGTGACA-3′	5′-AAGGGACTTCCTGTAACAATGCA-3′
HMBS	5′-GGCAATGCGGCTGCAA-3′	5′-GGGTACCCACGCGAATCAC-3′
B2M	5′-CGCTCCGTGGCCTTAGC-3′	5′-GAGTACGCTGGATAGCCTCCA-3′
HPRT	5′-GACCAGTCAACAGGGGACAT-3′	5′-AACACTTCGTGGGGTCCTTTTCAC-3′
cGAS	5′-TCACGTATGTACCCAGAACCC-3′	5′-CGCAGTTATCAAAGCAGAGGC-3′
STING	5′-TCAAGGATCGGGTTTACAGC-3′	5′-TGGCAAACAAAGTCTGCAAG-3′
IRF3	5′-CCCTTCATTGTAGATCTGATTACC-3′	5′-TGCAGGTCCACAGTATTCTC-3′
MX1	5′-GTTTCCGAAGTGGACATCGCA-3′	5′-CTGCACAGGTTGTTCTCAGC-3′
OAS1	5′-GAGCTCCAGGGCATACTGAG-3′	5′-CCAAGCTCAAGAGCCTCATC-3′
IFIT1	5′-CTCACATTTGCTTGGTTGTC-3′	5′-CAACCATGAGTACAAATGGTG-3′
IFIT2	5′-AGGTCTCTTCAGCATTTATTGG-3′	5′-TATTGTTCTCACTCATGGTTGC-3′
IFI44L	5′-AACTGTGGTATAGCATATGTGG-3′	5′-CTCTCAATTGCACCAGTTTCC-3′
ISG20	5′-GCTTGCCTTTCAGGAGCTG-3′	5′-ATCACCGATTACAGAACCCG-3′
CXCL10	5′-TGGCATTCAAGGAGTACCTC-3′	5′-TTGTAGCAATGATCTCAACACG-3′

Table S5. **Antibodies used in the study**

Antibody	Manufacturer	Description	Catalog number	Antibody dilution
Primary antibodies				
α-BLM	Abcam	Anti-BLM antibody (rabbit)	ab2179	1/5,000
α-Actin	Sigma-Aldrich	Anti-actin β antibody (Rabbit)	SAB5500001	1/10,000
α-GAPDH	Santa Cruz	Anti-GAPDH antibody (Mousse)	sc-32233	1/10,000
α-cGAS	Sigma-Aldrich	Anti-MB21D1 antibody (rabbit, Prestige antibody)	HPA031700	1/1,000
	Cell Signaling	cGAS (D1D3G) rabbit mAb	#15102	1/1,000
α-STING	Cell Signaling	STING (D2P2F) rabbit mAb	#13647	1/1,000
α-IRF3	IBL	Anti-human IRF-3 (IFN regulatory factor-3) rabbit IgG Affinity Purify	18781	1/1,000
α-MX1	Abcam	Anti-MX1 antibody (rabbit)	ab95926	1/1,000
α-MX2	Sigma-Aldrich	Anti-MX2 antibody (rabbit)	HPA030235-100UL	1/1,000
α-OAS1	Sigma-Aldrich	Anti-OAS1 antibody (rabbit, Prestige antibody)	HPA003657	1/1,000
α-IFIT1	Cell Signaling	IFIT1 antibody (rabbit)	12082S	1/1,000
α-TREX1	Abcam	Anti-TREX1 antibody (rabbit)	ab185228	1/1,000
Secondary antibodies				
α-Rabbit	Santa Cruz	Goat anti-rabbit HRP	sc-2054	1/5,000
α-Rabbit	Bethyl	Goat anti-rabbit IgG-heavy and light chain	A120-201P	1/5,000
α-Mouse	Santa Cruz	Goat anti-mouse HRP	sc-2055	1/5,000

Table S6. **Number of primary nuclei analyzed in imaging experiments**

Refers to	Experiment number	Conditions and number of nuclei	
Fig. 5 B		**EV**	**sgBLM**
	20171027	678	453
	20171102	310	222
	20171108	1,221	752
	20171112	1,248	1,222
	20180112	225	556
	20171103	765	448
	20180221	1,266	547
Fig. 5 C and Fig. S5 B		**EV**	**BLM**
	20171102	310	222
	20171108	1,221	752
	20180112	225	556
	20171123	141	187
	20171103	765	448
Fig. 5 D and Fig. S5 C		**CTRL**	**BLM**
	20181213	609	653
	20181217	353	539
	20181218.1	749	890
Fig. 5 E and Fig. S5 D		**EV**	**sgBLM**
	20181211	UT: 1,413	1,486
		APH: 846	611
	20181213	UT: 730	772
		APH: 549	622
	20181219	UT: 1,288	709
		APH: 700	571
	20181221	UT: 1,713	693
		APH: 706	526
	20190103	UT: 1,475	2,209
		APH: 1,226	1157
	20190107	UT: 716	732
		APH: 630	499
	20190110	UT: 1,588	1,787
		APH: 990	506
Fig. 5 F and Fig. S5 E		**EV**	**BLM**
	20181213	375	554
	20181217	643	674
	20181218.1	711	550
	20181218.2	420	675

APH, aphidicolin; sgBLM, single guide RNA against BLM; UT, untreated.

References

Lahkim Bennani-Belhaj, K., S. Rouzeau, G. Buhagiar-Labarchède, P. Chabosseau, R. Onclercq-Delic, E. Bayart, F. Cordelières, J. Couturier, and M. Amor-Guéret. 2010. The Bloom syndrome protein limits the lethality associated with RAD51 deficiency. *Mol. Cancer Res.* 8:385–394. https://doi.org/10.1158/1541-7786.MCR-09-0534

Schoggins, J.W., S.J. Wilson, M. Panis, M.Y. Murphy, C.T. Jones, P. Bieniasz, and C.M. Rice. 2011. A diverse range of gene products are effectors of the type I interferon antiviral response. *Nature.* 472:481–485. https://doi.org/10.1038/nature09907